Radiogenomic Analysis Demonstrates Associations between ^{18}F-Fluoro-2-Deoxyglucose PET, Prognosis, and Epithelial-Mesenchymal Transition in Non–Small Cell Lung Cancer[1]

Shota Yamamoto, MD
Danshan Huang, MD, PhD
Liutao Du, MD, PhD
Ronald L. Korn, MD, PhD
Neema Jamshidi, MD, PhD
Barry L. Burnette, PhD
Michael D. Kuo, MD

Purpose: To investigate whether non–small cell lung cancer (NSCLC) tumors that express high normalized maximum standardized uptake value (SUV_{max}) are associated with a more epithelial-mesenchymal transition (EMT)–like phenotype.

Materials and Methods: In this institutional review board–approved study, a public NSCLC data set that contained fluorine 18 (^{18}F) fluoro-2-deoxyglucose positron emission tomography (PET) and messenger RNA expression profile data (n = 26) was obtained, and patients were categorized on the basis of measured normalized SUV_{max} values. Significance analysis of microarrays was then used to create a radiogenomic signature. The prognostic ability of this signature was assessed in a second independent data set that consisted of clinical and messenger RNA expression data (n = 166). Signature concordance with EMT was evaluated by means of validation in a publicly available cell line data set. Finally, by establishing an in vitro EMT lung cancer cell line model, an attempt was made to substantiate the radiogenomic signature with quantitative polymerase chain reaction, and functional assays were performed, including Western blot, cell migration, glucose transporter, and hexokinase assays (paired t test), as well as pharmacologic assays against chemotherapeutic agents (half-maximal effective concentration).

Results: Differential expression analysis yielded a 14-gene radiogenomic signature ($P < .05$, false discovery rate [FDR] < 0.20), which was confirmed to have differences in disease-specific survival (log-rank test, $P = .01$). This signature also significantly overlapped with published EMT cell line gene expression data ($P < .05$, FDR < 0.20). Finally, an EMT cell line model was established, and cells that had undergone EMT differentially expressed this signature and had significantly different EMT protein expression ($P < .05$, FDR < 0.20), cell migration, glucose uptake, and hexokinase activity (paired t test, $P < .05$). Cells that had undergone EMT also had enhanced chemotherapeutic resistance, with a higher half-maximal effective concentration than that of cells that had not undergone EMT ($P < .05$).

Conclusion: Integrative radiogenomic analysis demonstrates an association between increased normalized ^{18}F fluoro-2-deoxyglucose PET SUV_{max}, outcome, and EMT in NSCLC.

Online supplemental material is available for this article.

[1] From the Department of Radiology, The David Geffen School of Medicine at University of California–Los Angeles (UCLA), 10833 LeConte Ave, Box 951721, CHS 17-135, Los Angeles, CA 90095-1721 (S.Y., D.H., L.D., N.J., B.L.B., M.D.K.); Department of Bioengineering, UCLA, Los Angeles, Calif (M.D.K.); and Scottsdale Medical Imaging, Scottsdale, Ariz (R.L.K.). Received February 1, 2016; revision requested February 11; revision received February 26; accepted March 4; final version accepted March 24. **Address correspondence to** M.D.K. (e-mail: *mikedkuo@gmail.com*).

Numerous studies have shown that the rate of fluorine 18 (^{18}F) fluoro-2-deoxyglucose (FDG) uptake, measured by using maximum standardized uptake value (SUV_{max}) in the primary tumor site, correlates with metastasis, resistance to chemotherapy, and poor overall clinical outcomes in non–small cell lung cancer (NSCLC) and other tumors (1–10). Interestingly, these same traits are also hallmarks of epithelial tumor cells that have undergone a characteristic change in molecular phenotype, known as epithelial-mesenchymal transition (EMT) (11,12). EMT is increasingly being recognized as a critical cancer phenotype in major tumor types, such as lung, breast, and colon cancer, and is associated with aggressive behavior, such as poor prognosis, chemotherapeutic resistance, and increased metastasis (11–15). Briefly, EMT is believed to be a conserved cellular developmental program associated with tissue morphogenesis during embryologic development that becomes "hijacked" in certain epithelial cancer cells, whereby the cells lose their apical-basal polarity and cell-cell contact inhibition and acquire a fibroblast-like morphology (16). Tumor cells that undergo EMT (hereafter referred to as "post-EMT" cells) express characteristic genes relative to tumor cells that do not undergo EMT (hereafter referred to as "pre-EMT" cells), including downregulation of epithelial-cadherin and upregulation of neural-cadherin, vimentin, matrix metallopeptidase-9, and versican, and ultimately acquire an aggressive phenotype functionally characterized by enhanced mobility, invasiveness, and chemoresistance (17–20). Indeed, a number of drugs are currently in development that aim to target and modulate this process, highlighting its increasingly appreciated role in cancer and tumor aggression (11). Given these shared phenotypic similarities between NSCLC tumors with high SUV_{max} and post-EMT cells, it is plausible that there may potentially be a link between these two processes. We hypothesized that NSCLC tumors expressing high normalized SUV_{max} are associated with a more EMT-like phenotype.

Advances in Knowledge

- A normalized fluorine 18 (^{18}F) fluoro-2-deoxyglucose (FDG) PET standardized uptake value (SUV) (maximum SUV [SUV_{max}] in the tumor/mean liver SUV) radiogenomic signature was derived in non–small cell lung cancer (NSCLC), which was prognostic in an independent gene expression data set ($P = .01$).
- This radiogenomic signature was significantly associated with epithelial-mesenchymal transition (EMT) in independent in vitro EMT cell line data ($P < .05$).
- An NSCLC EMT cell line was established that showed significant associations with increased cell migration, drug resistance, glucose uptake, and hexokinase activity ($P < .05$).

Materials and Methods

In this institutional review board–approved and Health Insurance Portability and Accountability Act–compliant study, we performed a multiphase, integrative radiogenomic analysis to investigate the relationship between FDG PET tumor standardized uptake value (SUV), outcomes, and EMT in NSCLC. Briefly, radiogenomics is a method for associating clinical imaging data with cellular and subcellular phenotypic information (21–29).

In the first phase, two independent publicly available NSCLC data sets from different institutions were accessed. Patient populations contained a combination of FDG PET images, messenger RNA (mRNA) expression data, or clinical outcomes data that could be used to construct an FDG PET–associated radiogenomic signature that defines relationships between imaging, mRNA expression, and clinical outcome. The second phase consisted of in silico analysis to evaluate any relationships between this radiogenomic signature and EMT. This was followed by the final phase, consisting of establishment of a lung cancer cell line model of EMT with subsequent confirmatory and functional analysis. The overall study design and organization are shown in Figure 1.

Implication for Patient Care

- NSCLC with high normalized SUV_{max} on ^{18}F-FDG PET images may be associated with EMT, which is implicated in metastasis and chemoresistance.

NSCLC ^{18}F FDG PET SUV Index Imaging Biomarker

Since tumor SUV_{max} estimates can be affected by intra- and interinstitutional variability, several investigators have recommended use of tumor SUV_{max} normalized to the mean liver SUV, referred to as "SUV_{index}," to control for variations; SUV_{index} has been shown by multiple investigators to be prognostic, such as in lung, liver, and head and neck cancers (30–33). We placed a constant circular region of interest diameter of 30 mm, averaged across three consecutive axial sections in the

Published online before print
10.1148/radiol.2016160259 **Content code:** CH

Radiology 2016; 280:261–270

Abbreviations:
EMT = epithelial-mesenchymal transition
FDG = fluoro-2-deoxyglucose
FDR = false discovery rate
mRNA = messenger RNA
NSCLC = non–small cell lung cancer
qPCR = quantitative polymerase chain reaction
SUV = standardized uptake value
SUV_{index} = SUV_{max} normalized to the mean liver SUV
SUV_{max} = maximum SUV
TGF-β = transforming growth factor β

Author contributions:
Guarantors of integrity of entire study, S.Y., M.D.K.; study concepts/study design or data acquisition or data analysis/interpretation, all authors; manuscript drafting or manuscript revision for important intellectual content, all authors; approval of final version of submitted manuscript, all authors; agrees to ensure any questions related to the work are appropriately resolved, all authors; literature research, S.Y., L.D., R.L.K., N.J., B.L.B., M.D.K.; clinical studies, S.Y., R.L.K.; experimental studies, S.Y., D.H., L.D., R.L.K., B.L.B., M.D.K.; statistical analysis, S.Y., L.D., N.J., M.D.K.; and manuscript editing, S.Y., L.D., R.L.K., N.J., B.L.B., M.D.K.

Conflicts of interest are listed at the end of this article.

Figure 1

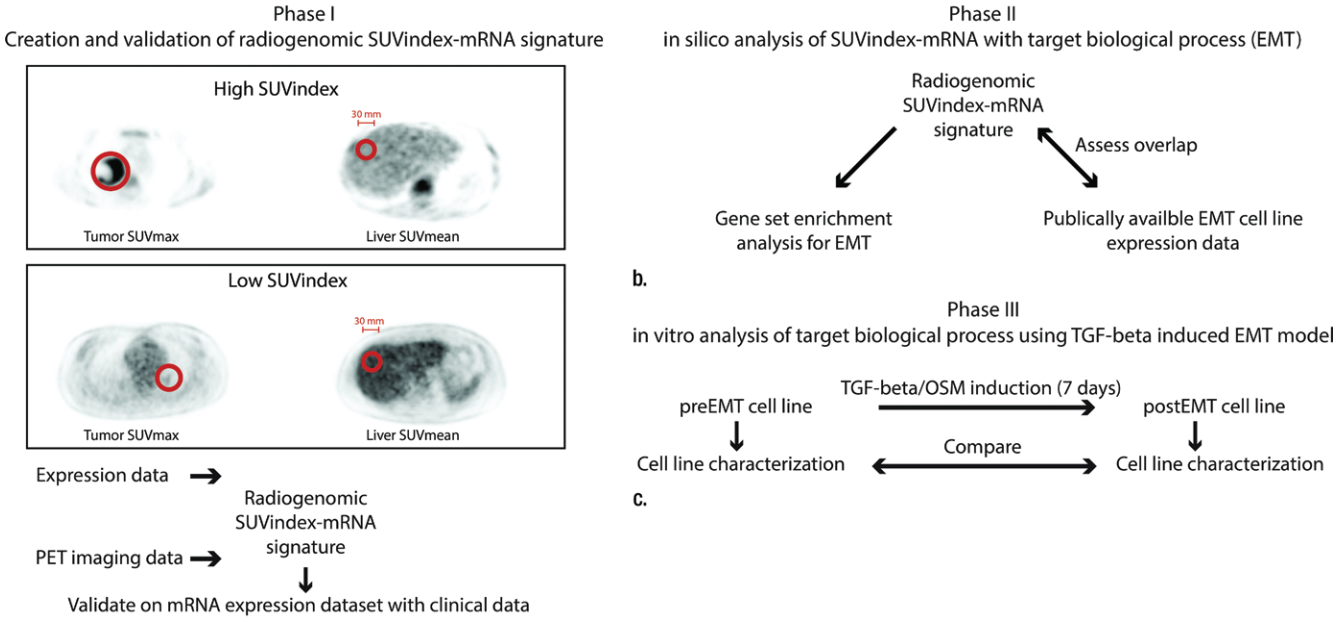

Figure 1: Flowcharts of overall study design, detailing **(a)** construction of the SUV_{index} mRNA radiogenomic signature (phase 1), **(b)** in silico analysis and assessment for biological associations of the SUV_{index} mRNA radiogenomic signature (phase 2), and **(c)** validation of the radiogenomic signature in an in vitro model (phase 3). *OSM* = oncostatin M.

anterior aspect of the right lobe of the liver, by using Osirix software (version 7.0; *http://www.osirix-viewer.com*) (34,35) as shown in Figure 1. All measurements and lesion identification were performed by a dual-certified nuclear medicine and radiology physician with 19 years of experience (R.L.K.) who was blinded to all clinical, pathologic, and genomic data. The ^{18}F FDG PET image acquisition parameters and protocol for data set 1 have been described previously: An ^{18}F FDG dose between 10 and 17 mCi (370 and 629 MBq, respectively; the dose was calculated on the basis of patient weight in kilograms) was administered, and imaging was performed by using a Discovery STE or LS PET/computed tomography scanner (GE Healthcare, Little Chalfont, United Kingdom) (36).

Phase 1: Radiogenomic Evaluation of SUV_{index}

SUV_{max} was measured for the same metabolically active lung tumor analyzed in the original study, as described previously, where examples are provided (data set 1, 26 patients with a histopathologic diagnosis of adenocarcinoma or squamous cell carcinoma, gene expression omnibus data set GSE28827) and normalized according to the mean SUV of the liver to convert the values to the SUV_{index}, which was the sole quantitative score used for all subsequent analysis (36). Patients were subsequently stratified into groups with high and low SUV_{index} scores by using a cutoff value based on the distribution of SUV_{index} scores (36,37). Matched mRNA expression data extracted from the SUV_{index}-quantified tumor lesion were filtered as described previously (36). Significance analysis of microarrays at a cutoff P value of less than .05 and a false discovery rate (FDR) of less than 0.20 by using 2000 permutations was used to generate the SUV_{index} mRNA radiogenomic signature (38,39).

Next, to confirm the prognostic power of our SUV_{index} mRNA signature, we applied this radiogenomic signature in an independent data set of 181 patients with NSCLC who had clinical and gene expression data (data set 2, gene expression omnibus data set GSE50081) (40). To match the patients to those in data set 1, only patients with a definitive histopathologic diagnosis of adenocarcinoma or squamous cell carcinoma were included (n = 170). Subsequently, after applying these criteria, four patients were excluded because of absence of clinical outcome data, which resulted in a subsequent analysis of a total of 166 of 181 patients (91.7%). Two-way average-linkage hierarchical clustering was performed on the SUV_{index} mRNA signature, with high and low SUV_{index} mRNA signature groups defined by taking the cutoff at the top node of the sample dendrogram. Both disease-specific survival and overall survival were assessed on the basis of differential expression of the SUV_{index} mRNA signature by using the log-rank test. Patient characteristics and statistical comparisons are described in Table 1.

Table 1

Data Sets

Data Set	mRNA and PET	mRNA and Survival	*P* Value*
Gene expression omnibus data set	GSE28827	GSE50081	…
Data set no.	1	2	…
No. of patients	26	166	…
Age (y)	Not available	41–88†	…
Patient sex			.04
No. of women	18	78	
No. of men	8	88	
Histologic finding			.81
Adenocarcinoma	20	124	
Squamous cell carcinoma	6	42	
Stage at diagnosis			.07
Stage I	20	51	
Stage II	3	115	
Stage III	2	0	
Stage IV	1	0	

* According to the unpaired *t* test, with unequal variance.

† Median age was 70 years.

Phase 2: Assessment of the SUV_{index} mRNA Expression Signature for Molecular Concordance and Associations with EMT

Gene set enrichment analysis was performed to evaluate any relationships between the SUV_{index} mRNA radiogenomic signature and EMT by using 20 curated EMT gene sets (Table E1 [online]) from the Molecular Signatures Database, with statistical significance set at *P* less than .05 and FDR less than 0.20. Finally, we evaluated the SUV_{index} mRNA signature against a publicly available cell line data set from a published in vitro EMT study (gene expression omnibus data set GSE49644) (41). Genes were extracted manually from the radiogenomic signature to compare the pre-EMT versus post-EMT cell expression values that were available in triplicate, in addition to calculation of the hypergeometric distribution. The *P* values were adjusted for multiple hypothesis testing by calculating the overall FDR across 14 genes by using the methods of Benjamini and Hochberg (39). *P* less than .05 and FDR less than 0.20 were considered to indicate statistically significant differences.

Phase 3: In Vitro Confirmation of Associations between SUV_{index} Radiogenomic Signature and EMT

Establishing an in vitro lung EMT model in a lung cancer cell line.—Detailed description of the cell line experiments performed in phase 3 can be found in Appendix E1 (online). Cell line induction and comparisons were performed in triplicates. All comparisons between pre-EMT and post-EMT cells in the subsequent analysis were performed by using a paired *t* test when comparing values obtained from each of the respective experiments.

Cell culture and cytokine treatment.—Briefly, the H358 lung cancer cell line was obtained from the American Type Culture Collection. Cells were grown according to protocol. To induce EMT, H358 cells were exposed to both transforming growth factor β (TGF-β, 10 ng/mL) and oncostatin M (50 ng/mL) (Cell Signaling Technology, Danvers, Mass) for 7 days.

Cells were collected and fractionated according to protocol (Bio-Rad, Hercules, Calif). After incubation, the membrane was washed and incubated with antibodies against human E-cadherin (1:1000), *n*-cadherin (1:1000), vimentin (1:2000), glucose transporter 1 (1:1000), hexokinase (1:1000), and actin (1:5000) (Cell Signaling).

Gene Expression Analysis by Using Quantitative Polymerase Chain Reaction

For both pre-EMT and post-EMT H358 RNA samples, expression analysis was performed by using an RNeasy purification kit (Qiagen, Valencia, Calif). Primers for quantitative polymerase chain reaction (qPCR) were designed and validated according to standard protocol (Table E2 [online]). Relative quantification values for each gene were calculated by using the δ threshold cycle method (42). Again, the *P* values were adjusted for multiple hypothesis testing by calculating the overall FDR across 14 genes (39). *P* less than .05 and FDR less than 0.20 were considered to indicate statistically significant differences. Hypergeometric probability was calculated to assess significance of overlap in directionality to the radiogenomic signature.

Cell Invasion Assay

Briefly, cell invasion was measured by using the CytoSelect 24-well cell migration and invasion assay (Cell Biolabs, San Diego, Calif) according to the manufacturer's instructions. Each sample was measured with optical density at 560 nm (BioTek, Winooski, Vt).

Comparison of Drug Response between Pre-EMT and Post-EMT Cells

Pre-EMT and post-EMT H358 cells were seeded to create 10-point dose-response curves for paclitaxel ($n = 6$) and mitoxantrone ($n = 9$) at increasing concentrations (0.0001–0.1 μmol/L). Cell viability was measured with the CellTiter-Glo Luminescent kit (Promega, Madison, Wis). Half-maximal effective concentration was calculated to measure differences between pre-EMT and post-EMT cells.

Glucose Uptake Assay

Briefly, pre-EMT and post-EMT cells in triplicates were incubated and grown according to the manufacturer's protocol (Cayman Chemical, Ann Arbor, Mich). The fluorescence was measured at 485 nm and 535 nm (43).

Hexokinase Activity Assay

Pre-EMT and post-EMT cell extracts were added to a reaction buffer in triplicate (Sigma-Aldrich, St Louis, Mo). The activity of hexokinase was determined by nicotinamide adenine dinucleotide formation after the absorbance at 340 nm and compared between two time points (0 minutes and 35 minutes).

Statistical Analysis

Expression data and survival analysis were performed with R version 3.0.1 *(http://www.R-project.org)* and SPSS (version 21.0; IBM, Armonk, NY) software. Cluster 3.0 and Java TreeView *(jtreeview.sourceforge.net)* were used for clustering analysis and visualization (44,45). Dose response curves were generated by using Prism (version 6.01; Graphpad, La Jolla, Calif).

Results

Phase 1: Defining the SUV_{index} mRNA Radiogenomic Signature and Evaluation of Its Clinical Concordance

A total of 48 778 measured genes in the array were filtered down to 1565 genes for subsequent analysis (HumanHT-12 version 3.0 expression beadchip; Illumina, San Diego, Calif). Optimal SUV_{index} cutoff into groups with high and low SUV_{index} values was set at 2.0 on the basis of the distribution of SUV_{index} values across all patients (low, n = 14; high, n = 12; Fig E1 [online]). Radiogenomic analysis was used to identify 14 genes differentially expressed in the group with high SUV_{index} scores relative to the group with low scores (Table 2); notable genes overexpressed in the high-SUV_{index} group included TGF-β–induced, matrix metallopeptidase-9, and versican, all of which have been strongly implicated in EMT.

We next verified the clinical significance of this SUV_{index} mRNA radiogenomic signature in data set 2 by stratifying the 166 patients into two discrete groups on the basis of their differential expression profile. The high-SUV_{index} group (n = 94) was associated with shorter disease-specific survival compared with the low-score group (n = 72; P = .01 according to the log-rank test; Fig 2). The median survival time was not reached by either group. Shorter overall survival was also observed in the high-SUV_{index} group (P = .045 according to the log-rank test, Fig E2 [online]). Comparison of the demographics among the two data sets did not show

Table 2

SUV_{index} mRNA Signature

Gene	*P* Value	Fold Change	FDR
PLAU	<.001	2.8	0.12
PGC	.001	−5.1	<0.01
SPP1	.002	2.9	0.12
TMEM158	.002	2.3	0.12
FASN	.002	−2.3	<0.01
VCAN	.003	2.4	0.12
PODXL2	.004	−2.3	<0.01
MXRA5	.004	2.4	0.12
MMP9	.005	2.8	0.12
TGFBI	.007	2	0.12
ALOX5AP	.008	2.3	0.12
CSF1R	.01	2.2	0.12
ITGB2	.01	2.3	0.12
RGS1	.01	2.0	0.12

Note.—MMP9 = matrix metallopeptidase-9, TGFBI = TGF-β–induced, VCAN = versican.

Figure 2

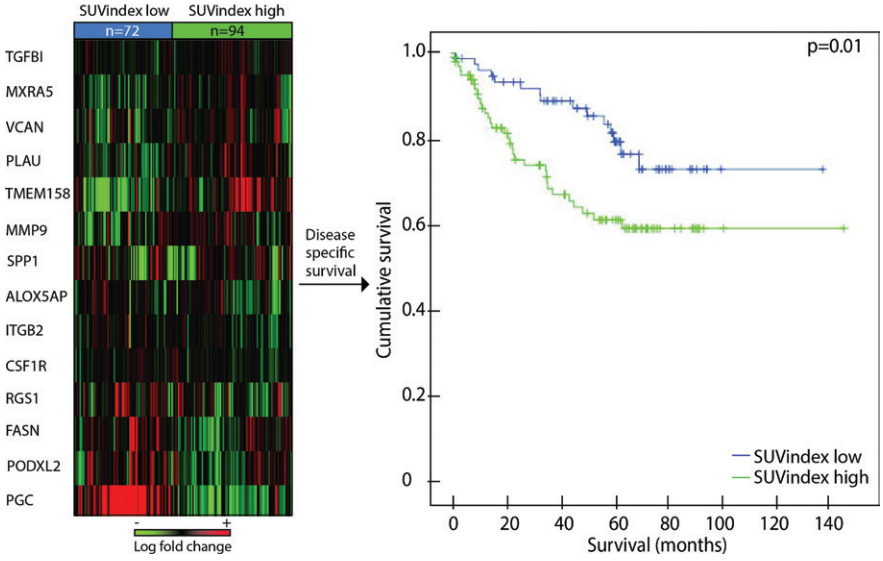

Figure 2: Heat map (left) and Kaplan-Meier survival curve (right) show the radiogenomic associations between SUV_{index}, mRNA expression, and clinical outcomes by leveraging independent data sets. The heat map shows the 14-gene signature with a relative expression reference below it (green = lower expression, red = higher expression); rows represent genes, and columns represent samples. The samples with relatively low expression levels for SUV_{index} are highlighted in blue and are denoted as *low*; samples with high expression levels are highlighted in green and are denoted as *high*. The SUV_{index} mRNA radiogenomic signature confirms differences in disease-specific survival (undefined median survival times for both groups) in 166 patients (P = .01, log-rank test). *MMP9* = matrix metallopeptidase-9, *TGFBI* = TGF-β–induced, *VCAN* = versican.

significant differences in the patient characteristics, except for patient sex (Table 1).

Phase 2: Assessment of the SUV_{index} mRNA Expression Signature for Molecular Concordance and Associations with EMT

At the mRNA level, gene set enrichment analysis of the SUV_{index} mRNA signature against 20 curated EMT-related gene sets in the Molecular Signatures Database (Table E1 [online]) was used to identify a significant association between the high SUV_{index} mRNA signature and "Jechlinger epithelial to mesenchymal transition up," a mesenchymal-like signature in a TGF-β–induced epithelial cell model of EMT ($P < .05$, FDR < 0.20). We performed additional validation of the association of our 14-gene signature with EMT on a publicly available data set (Human Genome U133 Plus 2.0 Array, 19849 transcripts; Affymetrix, Santa Clara, Calif), in which EMT induction was performed in three different lung cancer cell lines in triplicate (HCC827, A549, and H358). Overall, nine of 14 (64.3%), nine of 14 (64.3%), and 11 of 14 (78.6%) of the individual genes from the radiogenomic signature tested were significantly differentially expressed ($P < .05$, FDR $<$ 0.20) in the HCC827, A549, and H358 cell lines, respectively (Fig 3). Of the genes significantly expressed, seven of nine genes (77.8%), eight of nine genes (88.9%), and nine of 11 genes (81.8%), respectively, moved in the correct direction, confirming that the gene expression signatures were similar ($P < .0001$, hypergeometric probability; Fig 3).

Phase 3: In Vitro Confirmation of Radiogenomic Associations between the SUV_{index} Radiogenomic Signature and EMT

We next optimized a TGF-β and oncostatin M–based EMT induction approach as a means of inducing EMT in the H358 NSCLC cell line. A 7-day treatment of TGF-β and oncostatin M demonstrated significant changes toward mesenchymal morphology. Also, expected changes in in vitro expression of key EMT protein markers were seen; specifically, we observed downregulation of e-cadherin and upregulation of *n*-cadherin and vimentin according to Western blot analysis, which is consistent with previously reported studies (46). Migration assay repeated four times, as measured with fluorescence at an optical density of 560 nm, showed a fold change of 2.07 ± 047 ($P = .041$) in migration after EMT induction, confirming that post-EMT cells were more mobile than pre-EMT cells.

Next, to confirm the link between our 14-gene SUV_{index} mRNA radiogenomic signature and EMT in our model, we performed qPCR and differential expression analysis between the pre-EMT and post-EMT cells. qPCR confirmed concordant differential expression changes in 12 of 14 genes (85.7% at $P < .05$, FDR < 0.20; $P < .0001$, according to hypergeometric probability), thus confirming concordance in expression changes between our SUV_{index} mRNA signature and the EMT cell line.

To confirm the effect of EMT induction on drug resistance, we treated pre-EMT and post-EMT cells with two different chemotherapeutic agents (paclitaxel and mitoxantrone) at varying doses, and cell viability was assessed after treatment. Post-EMT cells were more resistant to both drugs when compared with pre-EMT cells on the basis of the half-maximal effective concentration values (paclitaxel, 0.005 μmol/L pre-EMT and 0.01 μmol/L post-EMT, $P < .001$; and mitoxantrone, 0.01 μmol/L pre-EMT and 0.03 μmol/L post-EMT, $P = .028$). All results are shown in Figure 4.

Finally, to confirm that post-EMT cells are also associated with increased

Figure 3

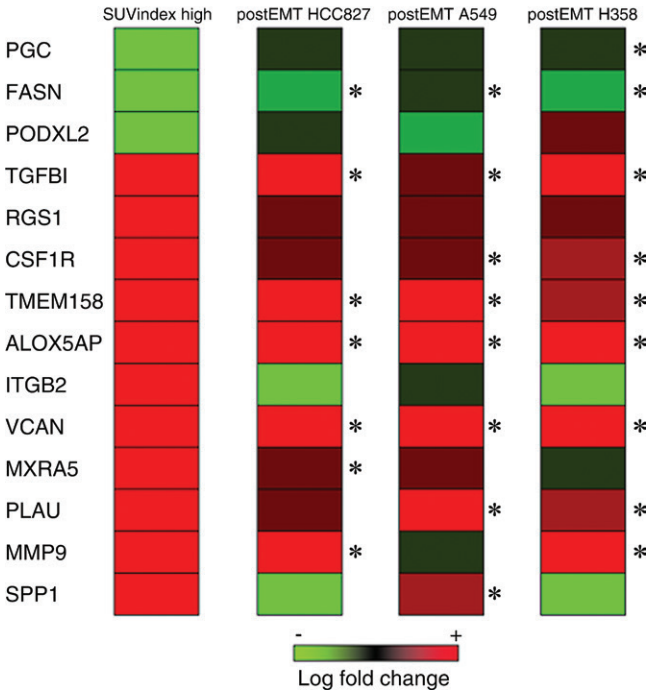

Figure 3: Heat map from in silico analysis confirms an association between the SUV_{index} mRNA signature and EMT. The heat map depiction (red is higher expression; green is lower expression) shows the concordance in expression levels between the SUV_{index} mRNA signature and expression levels from three different post-EMT experimental cell lines ($n = 3$ per cell line). * = genes with significantly different expression levels ($P < .05$, FDR < 0.20), which display similar direction in expression changes as the SUV_{index} mRNA signature. *MMP9* = matrix metallopeptidase-9, *TGFBI* = TGF-β–induced, *VCAN* = versican.

Figure 4

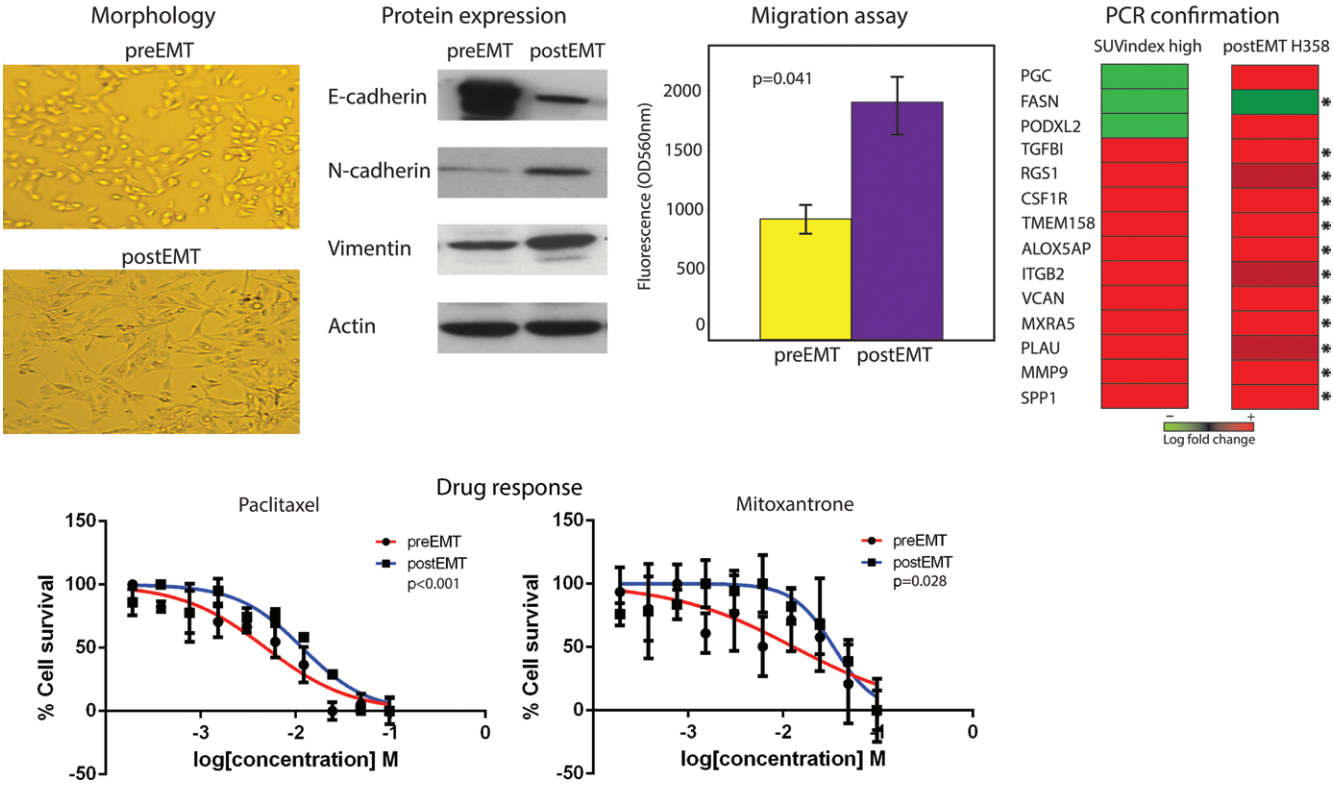

Figure 4: Photomicrographs (upper left), Western blot analysis (upper left center), bar graph (upper right center), heat map depiction (upper right), and plots (bottom) show qPCR and in vitro functional characterization to confirm association of the SUV_{index} mRNA signature with EMT and an aggressive cancer phenotype. On the photomicrographs (original magnification, ×10), characteristic changes in morphology are seen between pre-EMT and post-EMT H358 cells with light microscopy, which shows loss of cell-cell contact and appearance of elongated mesenchymal features, as well as confirmation of changes in EMT-associated protein markers. Cell migration assays confirm a significant increase in migration in post-EMT cells relative to pre-EMT H358 cells. The heat map (red is higher expression; green is lower expression) shows the concordance between the high SUV_{index} mRNA radiogenomic signature and gene expression of the post-EMT cells according to qPCR. * = genes with significantly different expression levels ($P < .05$, FDR < 0.20), which display similar direction in expression changes as the SUV_{index} mRNA signature. Nonlinear regression curves depict differences in cell survival (percentages) between the pre-EMT and post-EMT cells treated with paclitaxel and mitoxantrone at 10 different concentrations. There was a significant difference between the half-maximal effective concentration in both paclitaxel and mitoxantrone ($P < .001$ and $P = .028$, respectively). *MMP9* = matrix metallopeptidase-9, *TGFBI* = TGF-β–induced, *VCAN* = versican.

glucose uptake (as a surrogate for FDG uptake and higher SUV levels), we assayed both pre-EMT and post-EMT H358 cells for glucose uptake, with results presented in intensity values. Total fluorescence (435-nm and 535-nm) intensity values of 1123 ± 147 were observed for the pre-EMT cells, whereas post-EMT cells had total intensity values of 3703 ± 926 ($P = .001$, paired *t* test), representing a greater than threefold increase. Protein expression levels of both glucose transporter 1 and hexokinase also demonstrated increased expression in post-EMT cells compared with pre-EMT cells. Finally, the hexokinase activity assay also showed a significant increase of greater than 1.5-fold in activity in post-EMT cells (absorbance at 340 nm, 17.3 ± 0.10) relative to pre-EMT cells (11.2 ± 0.43) ($P = .003$, paired *t* test). All results are shown in Figure 5.

Discussion

There is a growing body of evidence highlighting the key role of EMT in aggressive cancers that include but are not limited to the lung, breast, pancreas, lymph nodes, and colon (15,47–50). Similarly, FDG PET imaging has been shown to not only be able to demonstrate lung cancers by depicting differences in glucose metabolism between tumor and nontumor cells but also allow differentiation of more aggressive lung tumors from less aggressive tumors on the basis of the degree of ^{18}F FDG uptake. Herein, using a multitiered radiogenomic approach with publicly available data sets in combination with our own in vitro studies, we provide evidence for an association in NSCLC between tumors that have high FDG uptake and EMT. We first identified and then validated an SUV mRNA radiogenomic signature in NSCLC by

Figure 5

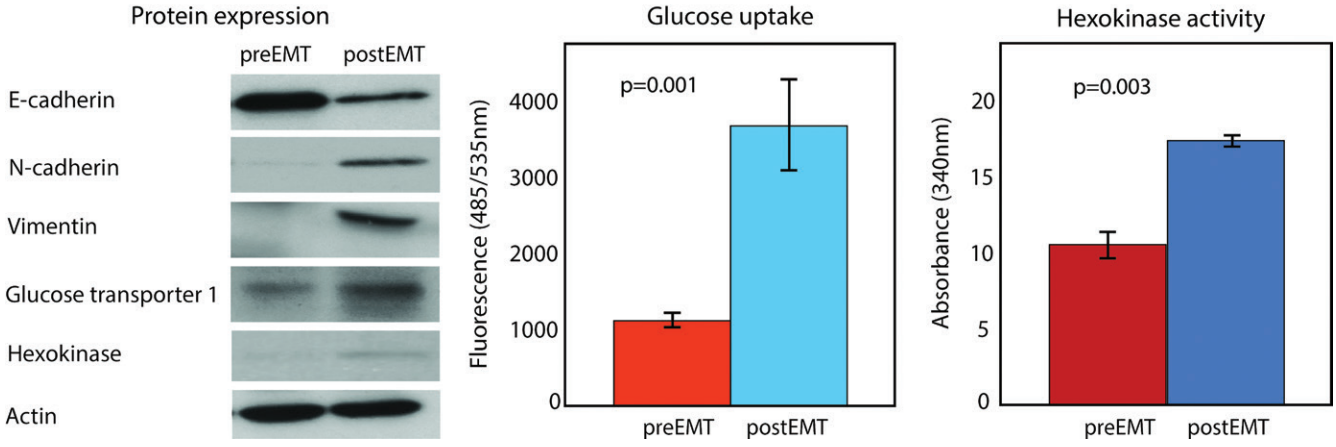

Figure 5: Western blot analysis (left) and bar graphs (rights) represent functional studies to confirm associations in glucose metabolism between EMT and SUV. Expression levels of glucose transporter 1 and hexokinase increases after EMT induction are shown. Glucose uptake increased 3.3-fold after EMT induction ($P < .001$). Hexokinase activity increased by nearly 1.5-fold in post-EMT cells ($P = .003$).

leveraging mRNA expression profile, clinical PET imaging, and clinical outcomes data. In silico analysis showed that this signature was associated with EMT both in a publicly available, experimental EMT lung cancer cell line model with gene expression data and through gene set enrichment analysis. To further confirm and characterize this link, we next established an inducible EMT model in an H358 NSCLC cell line. Having confirmed our EMT model, we performed functional characterization of pre-EMT versus post-EMT lung cancer cells to confirm the well-associated phenotypic changes associated with high-SUV NSCLC tumors, including demonstrating that post-EMT tumors had both increased migration and increased resistance to chemotherapeutic agents. Finally, we indirectly validated the potential relationship between SUV and EMT through a series of experiments that showed that post-EMT cells had significantly enhanced glucose transporter 1 mediated glucose uptake and hexokinase activity, as well as protein expression relative to that of pre-EMT lung cancer cells. Thus, by performing an integrative radiogenomic analysis by using independent data sets with imaging, outcomes, and gene expression in tandem with both in silico and functional in vitro analysis, we are able to provide multilevel biological support for an association between tumor SUV, poor outcome, and EMT in NSCLC.

Potential links between SUV and EMT have been suggested in several studies. One study showed that increased tumor SUV was associated with increased expression of several EMT-related genes in esophageal cancer; additionally, a number of investigators have shown in vitro that upregulation of glucose metabolism may play a role in EMT (51–54). One suggested mechanism is based on the effect of intratumoral upregulation of hypoxia inducible factor 1α, which has been shown to induce tumor invasion by triggering an EMT program by directly interacting with the key regulator twist family basic helix-loop-helix transcription factor 1 (53). In another study, EMT in breast cancer cells was shown to be activated by a metabolic switch to increased glucose metabolism (52). Although none of the transcripts in our SUV_{index} radiogenomic signatures are direct constituents of canonical glucose metabolism pathways, TGF-β is known to have powerful regulatory effects on glycolysis and gluconeogenesis. Additionally, our in vitro analysis confirmed significantly increased glucose uptake and glucose transporter 1 and hexokinase protein expression and activity in post-EMT H358 cells. Thus, our results suggest that NSCLC tumors with increased glucose metabolism as seen clinically with increased SUV_{index} are associated with EMT. Further studies will be necessary to confirm these findings and to further elucidate the molecular basis of these relationships.

Although EMT provides us with a potentially powerful lens with which to better understand the link between an important metabolic tumor image phenotype and its underlying behavior and biology, perhaps the real importance may derive from potential future clinical applications in guiding cancer therapy. Both de novo and acquired drug resistance continue to remain the major limitation for all cancer drugs; however, recent study findings are increasingly implicating EMT as a critical culprit in the chemoresistant phenotype. Recent studies in NSCLC, breast, and pancreatic cancer have shown that EMT serves as a critical determinant in eventual chemoresistance (55–57). In this work, we were able to further extend and characterize this relationship by demonstrating that post-EMT cells were not only more chemoresistant but that this chemoresistant population differentially expressed the high SUV_{index} mRNA radiogenomic signature when compared with the more chemosensitive tumors that expressed the low SUV_{index} radiogenomic signature. This is important because it has been shown that manipulating epithelial

plasticity through depletion of major EMT regulators can decrease drug resistance (58). Thus, it may be feasible to use FDG PET imaging to identify the lesions and populations of cells that are post-EMT and intrinsically resistant or have acquired chemoresistance and to then target them with either local or local-regional therapies or with next-generation drugs in current development that specifically target post-EMT–like cells.

One of the limitations of our study is that, although we provide multilevel evidence that links the EMT phenotype with the high-SUV tumor phenotype in NSCLC, we do not provide mechanistic studies. While this was not the goal of this study, future investigations could be directed toward elucidation of the molecular mechanisms at play that may be driving this multiscale phenotype. Further studies in larger clinical data sets with patient-derived cell lines could also strengthen the study and further confirm and extend our findings. Additionally, while FDR correction was applied to the qPCR differential expression analysis in phase 3 of this study, the remaining comparisons were analyzed by using a paired *t* test. Nonetheless, our results provide a strong basis, we believe, for further investigations and improved understanding of the relationships between multiscale imaging, clinical data, and cellular and subcellular phenotypes.

In conclusion, studies such as this, in which different data types are combined from different domains to address specific hypothesis-driven questions, will likely be important in future studies as a means to aid in the delineation of complex cancer phenotypes and their mechanisms of action, drug development, and identification of clinically useful biomarkers. By using such an approach, our integrative radiogenomic analysis demonstrates an association between increased normalized ^{18}F FDG PET SUV_{max}, outcome, and EMT in NSCLC.

Disclosures of Conflicts of Interest: S.Y. disclosed no relevant relationships. **D.H.** disclosed no relevant relationships. **L.D.** disclosed no relevant relationships. **R.L.K.** disclosed no relevant relationships. **N.J.** disclosed no relevant relationships. **B.L.B.** disclosed no relevant relationships. **M.D.K.** disclosed no relevant relationships.

References

1. Fischer B, Lassen U, Mortensen J, et al. Preoperative staging of lung cancer with combined PET-CT. N Engl J Med 2009;361(1):32–39.
2. Vander Heiden MG, Cantley LC, Thompson CB. Understanding the Warburg effect: the metabolic requirements of cell proliferation. Science 2009;324(5930):1029–1033.
3. de Geus-Oei LF, van Krieken JH, Aliredjo RP, et al. Biological correlates of FDG uptake in non–small cell lung cancer. Lung Cancer 2007;55(1):79–87.
4. Demura Y, Tsuchida T, Ishizaki T, et al. 18F-FDG accumulation with PET for differentiation between benign and malignant lesions in the thorax. J Nucl Med 2003;44(4):540–548.
5. Hutchings M, Loft A, Hansen M, et al. FDG-PET after two cycles of chemotherapy predicts treatment failure and progression-free survival in Hodgkin lymphoma. Blood 2006;107(1):52–59.
6. Kostakoglu L, Goldsmith SJ. 18F-FDG PET evaluation of the response to therapy for lymphoma and for breast, lung, and colorectal carcinoma. J Nucl Med 2003;44(2):224–239.
7. Dose Schwarz J, Bader M, Jenicke L, Hemminger G, Jänicke F, Avril N. Early prediction of response to chemotherapy in metastatic breast cancer using sequential 18F-FDG PET. J Nucl Med 2005;46(7):1144–1150.
8. Choi H, Charnsangavej C, Faria SC, et al. Correlation of computed tomography and positron emission tomography in patients with metastatic gastrointestinal stromal tumor treated at a single institution with imatinib mesylate: proposal of new computed tomography response criteria. J Clin Oncol 2007;25(13):1753–1759.
9. Berghmans T, Dusart M, Paesmans M, et al. Primary tumor standardized uptake value (SUVmax) measured on fluorodeoxyglucose positron emission tomography (FDG-PET) is of prognostic value for survival in non-small cell lung cancer (NSCLC): a systematic review and meta-analysis (MA) by the European Lung Cancer Working Party for the IASLC Lung Cancer Staging Project. J Thorac Oncol 2008;3(1):6–12.
10. Cerfolio RJ, Bryant AS, Ohja B, Bartolucci AA. The maximum standardized uptake values on positron emission tomography of a non–small cell lung cancer predict stage, recurrence, and survival. J Thorac Cardiovasc Surg 2005;130(1):151–159.
11. Singh A, Settleman J. EMT, cancer stem cells and drug resistance: an emerging axis of evil in the war on cancer. Oncogene 2010;29(34):4741–4751.
12. Kang Y, Massagué J. Epithelial-mesenchymal transitions: twist in development and metastasis. Cell 2004;118(3):277–279.
13. Polyak K, Weinberg RA. Transitions between epithelial and mesenchymal states: acquisition of malignant and stem cell traits. Nat Rev Cancer 2009;9(4):265–273.
14. Burk U, Schubert J, Wellner U, et al. A reciprocal repression between ZEB1 and members of the miR-200 family promotes EMT and invasion in cancer cells. EMBO Rep 2008;9(6):582–589.
15. Ma L, Teruya-Feldstein J, Weinberg RA. Tumour invasion and metastasis initiated by microRNA-10b in breast cancer. Nature 2007;449(7163):682–688.
16. Kalluri R. EMT: when epithelial cells decide to become mesenchymal-like cells. J Clin Invest 2009;119(6):1417–1419.
17. De Craene B, Berx G. Regulatory networks defining EMT during cancer initiation and progression. Nat Rev Cancer 2013;13(2):97–110.
18. Cicchini C, Laudadio I, Citarella F, et al. TGFbeta-induced EMT requires focal adhesion kinase (FAK) signaling. Exp Cell Res 2008;314(1):143–152.
19. Mani SA, Guo W, Liao MJ, et al. The epithelial-mesenchymal transition generates cells with properties of stem cells. Cell 2008;133(4):704–715.
20. Soltermann A, Tischler V, Arbogast S, et al. Prognostic significance of epithelial-mesenchymal and mesenchymal-epithelial transition protein expression in non–small cell lung cancer. Clin Cancer Res 2008;14(22):7430–7437.
21. Jamshidi N, Jonasch E, Zapala M, et al. The radiogenomic risk score: construction of a prognostic quantitative, noninvasive image-based molecular assay for renal cell carcinoma. Radiology 2015;277(1):114–123.
22. Jamshidi N, Jonasch E, Zapala M, et al. The radiogenomic risk score stratifies outcomes in a renal cell cancer phase 2 clinical trial. Eur Radiol 2015 Nov 11. [Epub ahead of print]
23. Yamamoto S, Maki DD, Korn RL, Kuo MD. Radiogenomic analysis of breast cancer using MRI: a preliminary study to define the landscape. AJR Am J Roentgenol 2012;199(3):654–663.
24. Yamamoto S, Korn RL, Oklu R, et al. ALK molecular phenotype in non–small cell lung cancer: CT radiogenomic characterization. Radiology 2014;272(2):568–576.

25. Yamamoto S, Han W, Kim Y, et al. Breast cancer: radiogenomic biomarker reveals associations among dynamic contrast-enhanced MR imaging, long noncoding RNA, and metastasis. Radiology 2015;275(2):384–392.

26. Jamshidi N, Diehn M, Bredel M, Kuo MD. Illuminating radiogenomic characteristics of glioblastoma multiforme through integration of MR imaging, messenger RNA expression, and DNA copy number variation. Radiology 2014;270(1):1–2.

27. Segal E, Sirlin CB, Ooi C, et al. Decoding global gene expression programs in liver cancer by noninvasive imaging. Nat Biotechnol 2007;25(6):675–680.

28. Diehn M, Nardini C, Wang DS, et al. Identification of noninvasive imaging surrogates for brain tumor gene-expression modules. Proc Natl Acad Sci U S A 2008;105(13):5213–5218.

29. Kuo MD, Gollub J, Sirlin CB, Ooi C, Chen X. Radiogenomic analysis to identify imaging phenotypes associated with drug response gene expression programs in hepatocellular carcinoma. J Vasc Interv Radiol 2007;18(7):821–831.

30. Lee JW, Paeng JC, Kang KW, et al. Prediction of tumor recurrence by 18F-FDG PET in liver transplantation for hepatocellular carcinoma. J Nucl Med 2009;50(5):682–687.

31. Imsande HM, Davison JM, Truong MT, et al. Use of 18F-FDG PET/CT as a predictive biomarker of outcome in patients with head-and-neck non–squamous cell carcinoma. AJR Am J Roentgenol 2011;197(4):976–980.

32. Shiono S, Abiko M, Okazaki T, Chiba M, Yabuki H, Sato T. Positron emission tomography for predicting recurrence in stage I lung adenocarcinoma: standardized uptake value corrected by mean liver standardized uptake value. Eur J Cardiothorac Surg 2011;40(5):1165–1169.

33. Shiono S, Yanagawa N, Abiko M, Sato T. Noninvasive differential diagnosis of pulmonary nodules using the standardized uptake value index. Ann Thorac Cardiovasc Surg 2015;21(3):236–241.

34. Laffon E, Marthan R. Interim FDG PET scans in lymphoma: SUV measurement error may impair qPET methodology. Eur J Nucl Med Mol Imaging 2014;41(11):2154.

35. Park HH, Park DS, Kweon DC, et al. Intercomparison of 18F-FDG PET/CT standardized uptake values in Korea. Appl Radiat Isot 2011;69(1):241–246.

36. Gevaert O, Xu J, Hoang CD, et al. Non–small cell lung cancer: identifying prognostic imaging biomarkers by leveraging public gene expression microarray data—methods and preliminary results. Radiology 2012;264(2):387–396.

37. Nair VS, Gevaert O, Davidzon G, et al. Prognostic PET 18F-FDG uptake imaging features are associated with major oncogenomic alterations in patients with resected non–small cell lung cancer. Cancer Res 2012;72(15):3725–3734.

38. Tusher VG, Tibshirani R, Chu G. Significance analysis of microarrays applied to the ionizing radiation response. Proc Natl Acad Sci U S A 2001;98(9):5116–5121.

39. Benjamini Y, Hochberg Y. Controlling the false discovery rate: a practical and powerful approach to multiple testing. J R Stat Soc Series B Stat Methodol 1995;57(1):289–300.

40. Der SD, Sykes J, Pintilie M, et al. Validation of a histology-independent prognostic gene signature for early-stage, non–small-cell lung cancer including stage IA patients. J Thorac Oncol 2014;9(1):59–64.

41. Sun Y, Daemen A, Hatzivassiliou G, et al. Metabolic and transcriptional profiling reveals pyruvate dehydrogenase kinase 4 as a mediator of epithelial-mesenchymal transition and drug resistance in tumor cells. Cancer Metab 2014;2(1):20.

42. Schmittgen TD, Livak KJ. Analyzing real-time PCR data by the comparative C(T) method. Nat Protoc 2008;3(6):1101–1108.

43. Zou C, Wang Y, Shen Z. 2-NBDG as a fluorescent indicator for direct glucose uptake measurement. J Biochem Biophys Methods 2005;64(3):207–215.

44. de Hoon MJ, Imoto S, Nolan J, Miyano S. Open source clustering software. Bioinformatics 2004;20(9):1453–1454.

45. Saldanha AJ. Java TreeView—extensible visualization of microarray data. Bioinformatics 2004;20(17):3246–3248.

46. Gill BJ, Gibbons DL, Roudsari LC, et al. A synthetic matrix with independently tunable biochemistry and mechanical properties to study epithelial morphogenesis and EMT in a lung adenocarcinoma model. Cancer Res 2012;72(22):6013–6023.

47. Lynch TJ, Bell DW, Sordella R, et al. Activating mutations in the epidermal growth factor receptor underlying responsiveness of non–small-cell lung cancer to gefitinib. N Engl J Med 2004;350(21):2129–2139.

48. Yauch RL, Januario T, Eberhard DA, et al. Epithelial versus mesenchymal phenotype determines in vitro sensitivity and predicts clinical activity of erlotinib in lung cancer patients. Clin Cancer Res 2005;11(24 Pt 1):8686–8698.

49. Rhim AD, Mirek ET, Aiello NM, et al. EMT and dissemination precede pancreatic tumor formation. Cell 2012;148(1-2):349–361.

50. Sánchez-Tilló E, Fanlo L, Siles L, et al. The EMT activator ZEB1 promotes tumor growth and determines differential response to chemotherapy in mantle cell lymphoma. Cell Death Differ 2014;21(2):247–257.

51. Kajiwara T, Hiasa Y, Nishina T, et al. Maximum standardized uptake value in (18) F-fluoro-2-deoxyglucose positron emission tomography is associated with advanced tumor factors in esophageal cancer. Mol Clin Oncol 2014;2(2):313–321.

52. Cannito S, Novo E, Compagnone A, et al. Redox mechanisms switch on hypoxia-dependent epithelial-mesenchymal transition in cancer cells. Carcinogenesis 2008;29(12):2267–2278.

53. Yang MH, Wu MZ, Chiou SH, et al. Direct regulation of TWIST by HIF-1α promotes metastasis. Nat Cell Biol 2008;10(3):295–305.

54. Guillaumond F, Leca J, Olivares O, et al. Strengthened glycolysis under hypoxia supports tumor symbiosis and hexosamine biosynthesis in pancreatic adenocarcinoma. Proc Natl Acad Sci U S A 2013;110(10):3919–3924.

55. Fischer KR, Durrans A, Lee S, et al. Epithelial to mesenchymal transition is not required for breast to lung metastasis but contributes to chemoresistance. Cancer Res 2015;75(15 Supplement):4721.

56. Fischer KR, Durrans A, Lee S, et al. Epithelial-to-mesenchymal transition is not required for lung metastasis but contributes to chemoresistance. Nature 2015;527(7579):472–476.

57. Zheng X, Carstens JL, Kim J, et al. Epithelial-to-mesenchymal transition is dispensable for metastasis but induces chemoresistance in pancreatic cancer. Nature 2015;527(7579):525–530.

58. Meng F, Speyer CL, Zhang B, et al. PDGFRα and β play critical roles in mediating Foxq1-driven breast cancer stemness and chemoresistance. Cancer Res 2015;75(3):584–593.